Reig Cerdá, L.; Amigó Borrás, V.; Busquets Mataix, DJ.; Calero, JA.; Ortiz Rosales, JL. (2012). Application of the Zero-Order Reaction Rate Model and Transition State Theory to predict porous Ti6Al4V bending strength. Materials Science and Engineering: C. 32(6):1621-1626. doi:10.1016/j.msec.2012.04.052.

Graphical Abstract

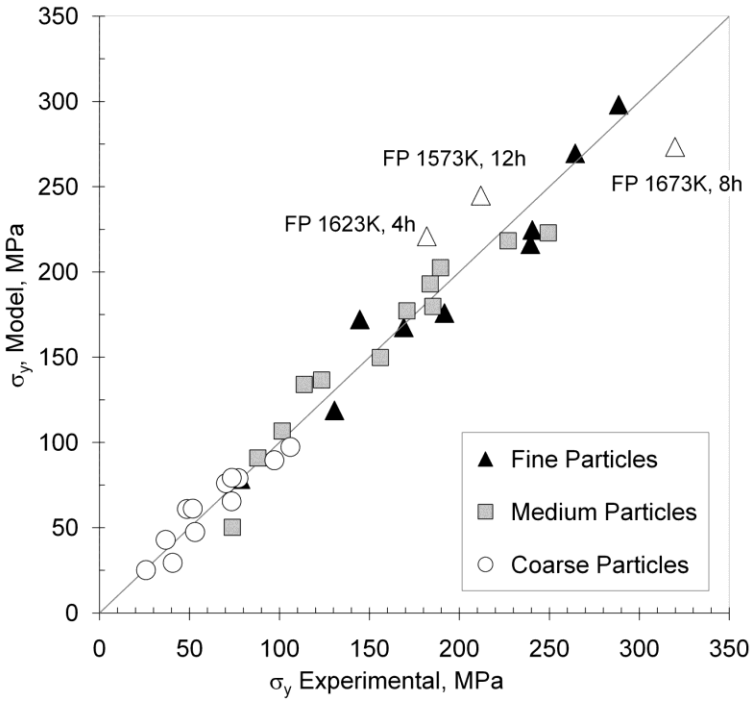

Titanium stiffness has been reduced producing porous specimens by means of microsphere sintering. Mathematical models are not suitable to model the sintering process of the present study, as they are based in parameters such as density, shrinkage or porosity, which vary very little in the porous samples developed. The zero-order reaction rate model (ZORR) and Transition State Theory (TST) were therefore used as an alternative method to model the sintering process and estimate bending strength of porous Ti6Al4V obtained by microsphere sintering. Although the model parameters have been obtained only for the microsphere sizes analyzed, the strength of intermediate sizes could be easily estimated following this model.

Research Highlights:

- A simple mathematical model based on the Zero Order Reaction Rate (ZORR) and Transition State Theory (TST) has been established to estimate bending strength of porous Ti6Al4V developed by microsphere sintering.

- Although the model parameters have been obtained only for the microsphere sizes analyzed, the strength of other sizes could be easily estimated following this model.

Application of the Zero-Order Reaction Rate model and Transition State Theory to predict porous Ti6Al4V bending strength

L. REIG[a], V. AMIGÓ[b], D. BUSQUETS[b] , J.A. CALERO[c], J.L. ORTIZ[d]

[a] Departamento de Ingeniería Mecánica y Construcción, Universitat Jaume I, Castelló. Av. de Vicent Sos Baynat, s/n, 12071 Castelló de la Plana, Spain

[b] Departamento de Ingeniería Mecánica y de Materiales, Universidad Politécnica de Valencia, Camino de Vera s/n, 46022 Valencia, Spain

[c] AMES, C\ Laureà Miró, 388. Sant Feliu de Llobregat, 08980 Barcelona, Spain

[d] Departamento de Mecatrónica, Instituto Tecnológico y de Estudios Superiores de Monterrey, Campus Querétaro, Epigmenio González 500, 76130 Santiago de Querétaro, Mexico

---

Corresponding author: L. Reig; Phone: +34 964 729163
E-mail address: lreig@emc.uji.es; vamigo@mcm.upv.es; dbusquets@mcm.upv.es; jacalero@ames.es; jlortiz@itesm.mx

ABSTRACT

Porous Ti6Al4V samples were produced by microsphere sintering. The Zero-Order Reaction Rate model and Transition State Theory were used to model the sintering process and to estimate the bending strength of the porous samples developed. The evolution of the surface area during the sintering process was used to obtain sintering parameters (sintering constant, activation energy, frequency factor, constant of activation and Gibbs energy of activation). These were then correlated with the bending strength in order to obtain a simple model with which to estimate the evolution of the bending strength of the samples when the sintering temperature and time are modified: $\sigma_Y = P + B \cdot \left[\ln(T \cdot t) - \frac{\Delta G_a}{R \cdot T} \right]$. Although the sintering parameters were obtained only for the microsphere sizes analysed here, the strength of intermediate sizes could easily be estimated following this model.

Key words: Porous Ti6Al4V, microsphere sintering, zero-order reaction rate model, surface area, bending strength.

1. Introduction

Titanium alloys exhibit an excellent combination of properties for use in biomedical applications [1-4]. For instance, their elastic modulus is lower than that presented by other metallic materials commonly used as implants, such as stainless steel and cobalt-chromium alloys (Ti6Al4V ≈ 110 GPa; Cr-Co-Mo ≈ 200-230 GPa; Stainless steel ≈ 200 GPa) [5-9]. Nevertheless, their stiffness is still excessive when compared to that of human cortical bone (10-30 GPa) [7,8] and this, according to Ysander [9], causes weakening problems that can lead to the loosening of the implant [9]. This problem has led researchers to look for different means of reducing the stiffness of titanium [8,10-13]. Some of the techniques that have been investigated are based on the development of porous structures, which have been reported to improve cell attachment when an appropriate degree of porosity and pore size are provided [11,14]. Regarding the procedures used to developed porous titanium structures, solid-phase sintering techniques have been proved to be more suitable than liquid-phase foaming. This is mainly due to the high melting point of titanium and its reactivity at high temperatures [5,14]. The porous samples used in this work were therefore developed by microsphere sintering.

Although different mathematical models have been proposed to obtain the kinetic activity parameters of the sintering process, they are all based on properties such as density, shrinkage rate or porosity and none of them show a high degree of variation during the sintering process used to produce the porous samples [15]. Other models, such as that based on the neck-growth sintering rate (NGSR) [16,17] or the nth-order Gaussian energy distribution model (NOGD) [18], have also been widely used for determining the sintering rate. Nevertheless, they too are based on shrinkage and density variations, as well as being complex and cumbersome to use. Authors such as Sarikaya et al. [15] satisfactorily employed the Zero-Order Reaction Rate (ZORR) model and Transition State Theory (TST) as an alternative to the aforementioned complex mathematical models.

The aim of the present research is to estimate the bending strength of porous Ti6Al4V samples produced by microsphere sintering by applying a ZORR model and TST.

2. Experimental

2.1. Raw material

Ti6Al4V alloy microspheres produced by the plasma rotating electrode process (PREP) were used to develop the porous specimens. Three different particle sizes were supplied by Phelly Materials Inc., who provided their chemical composition (Table I) and granulometric distribution (Figure 1). They have been referenced as Fine (FP), Medium (MP) and Coarse (CP) in this paper. Figure 2 shows their regular, spherical shape.

Apparent and Tap density of each microsphere size were determined according to ASTM B213-97 standards using a Hall flowmeter. The bulk density of Ti6Al4V was considered to have a value of 4.42 g/cm^3. In order to analyse the evolution of the surface area during the sintering process, the initial surface area per mass unit (S_0, m^2/g) was determined. It was calculated for every particle size distribution (FP, MP, CP) as the product between the surface area of an individual microsphere and the number of microspheres per mass unit. Due to the relatively narrow particle size distributions, the diameter adopted for the calculations was the average value of each particle fraction, namely 188.32 (FP), 219.65 (MP) and 457.67 (CP) μm (Figure 1). Tap density was found to be close to 2.81 g/cm^3 for all sizes.

2.2. Microsphere consolidation

Microspheres were sintered on yttria, following the process reported in [19]. As explained [19], because bulk yttria moulds are difficult to produce, alumina moulds were used as a support for the yttria coating. Despite reactivity being minimal when yttria was used as the mould material for microsphere sintering, some reactivity with the alumina substrate through the yttria coating was observed. Nevertheless, it was significant only when the smaller microspheres were sintered at higher temperatures (1400 ºC) or for longer times (8–12h) [19-21].

Sintering was performed at three different temperatures (1573K, 1623K and 1673K) for times ranging from 30 to 720 minutes (0.5 to 12h). As shown in Table II, some temperature-time combinations were not used, namely 1573K-30min and 1673K-720min. While the former was avoided because low bending strength values were expected, the latter was not used in order to prevent reactivity.

2.3. Three-point bending test

Bending strength was determined by the three-point bending test in accordance with ISO 3325:2000 (ASTM E290-97a). Rectangular samples (25 x 12 x 4 mm^3) were tested at a cross speed of 0.5 mm/s in an Instron 4204 Universal Testing machine.

2.4. Porosity, sinter neck and final surface area

Porosity was determined by the Archimedes method in compliance with Standard UNE EN ISO 2738:1999 (ASTM B328:2003) using a KERN 770 electronic microbalance and Sartorius YDK01 equipment.

The size of the necks developed between particles during the sintering process was determined for every condition (see Table II) after analysing SEM micrographs. An average size of the neck ($\varnothing_{NECK}$) was established as the average value of forty-five measurements. To take the measurements, sinter necks were considered to be circular, as they had a regular shape. For this reason, the diameter of the sinter neck developed was assumed to be the largest axis of the apparent ellipse obtained in the two-dimensional image (see Figure 3).

The surface area after sintering (S) was calculated as the difference between the initial surface area (S_0) and the neck area developed during the sintering process (N_{AREA}). Neck area per mass unit was calculated as the product between the neck area developed by one microsphere and the number of microspheres per gram. For one microsphere, the neck area was obtained by multiplying the area of a single neck ($\pi \cdot \phi_{NECK}^{\,2} / 4$) by the number of contacts between neighbouring microspheres (coordination index, CI).

In order to establish the CI, porosity results were analysed. Total porosity obtained by the Archimedes method ranged between 23% and 29%, regardless of the initial size of the microspheres and the sintering cycle applied. Therefore, porosity values are close to those of theoretical close-compact structures, with a packing factor of 0.74 (26% porosity) and a CI of 12 [22]. Nevertheless, in order to consider the particle-size distribution pattern, together with some degree of random arrangement in the mould, a slightly lower coordination index (CI = 10) was adopted.

3. Results

3.1. Application of the ZORR model

Figure 3 shows a porous Ti6Al4V micrograph after the sintering process. As can be seen, necks between particles are discernible and single microspheres can be clearly distinguished, thereby indicating that the sintering process is in the first stage [17]. A smaller variation in density or shrinkage was observed during the sintering process, which, according to German [23], is due to a reduced contribution of the volume diffusion mechanism to neck growth.

As reported in Table II, evolution of the surface area during sintering ($\Delta S/S_0 = (S_0 - S)/S_0$) was lower than 0.5, which, according to Sarikaya [15], allows the rate of sintering to be calculated by means of the evolution of the surface area. Higher variations were observed when sintering either at higher temperatures or smaller microspheres, which indicates a higher development of the N_{AREA}. Apparently this is in contradiction with the evolution of the $\varnothing_{NECK}$ value, which increases with the size of the microspheres for a given temperature-time cycle, as observed in Figure 4. Nevertheless, the evolution of N_{AREA} in the opposite way is explained by the greater specific surface area of the smaller microspheres, which (despite developing a smaller $\varnothing_{NECK}$) have a higher number of contact points among neighbouring microspheres.

3.2. Relation between surface area and bending strength

According to Sarikaya [15], the surface area after sintering can be related with sintering time by the zero-order equation (1):

$$S = S_0 - k \cdot t \tag{1}$$

where S_0 is the initial surface area, k the sintering constant and t the sintering time in minutes. From Figure 5 it holds that equation (1) fits well for shorter sintering times, deviating as the sintering time increases (720 min), probably due to reactivity with the alumina substrate of the mould [19]. Initial surface area, S_0, obtained graphically from Figure 5 (approximately $97 \cdot 10^{-4}$ m^2/g in FP, $85 \cdot 10^{-4}$ m^2/g in MP and $44 \cdot 10^{-4}$ m^2/g in CP), increases as microsphere size decreases. This is due to the larger specific surface area.

The sintering constant, k, can be related with the neck area developed while sintering by means of Equation 2:

$$S_0 - S = k \cdot t \rightarrow S_0 - \left(S_0 - N_{AREA}\right) = k \cdot t \rightarrow N_{AREA} = k \cdot t \tag{2}$$

In Figure 6, N_{AREA} (obtained through equation 2) is correlated with experimental bending strength values by means of a logarithmic model. Although a good fit was observed, some points show a high deviation (empty triangles in Figure 6). These points correspond to the smaller particles (FP) sintered at 1573K (1300 ºC) for 720 minutes and 1673K (1400 ºC) for 480 minutes. As previously reported [19], these anomalous values are related to some degree of reaction with the alumina substrate of the mould through the yttria coating. This happens mainly when sintering the smallest microspheres at high temperatures for long sintering times.

3.3. Estimation of sintering parameters

The sintering constant, *k*, was related to the sintering temperature through the Arrhenius Equation (3). To do so, constant 'k' units ($m^2g^{-1}min^{-1}$) were converted into $m^2mol^{-1}s^{-1}$ using the molar mass of Ti6Al4V alloy (413.54 mol^{-1}).

$$\ln(k) = \ln(A) - \frac{E_a}{R}\cdot\left(\frac{1}{T}\right) \tag{3}$$

where *R* is the ideal gas constant (8.314 $J\cdot K^{-1}mol^{-1}$), *T* is the sintering temperature in K, E_a is the activation energy and *A* the frequency factor. Although a higher number of experimental points would be desirable to achieve greater accuracy, it did allow us to estimate E_a and *A* for each microsphere size (FP, MP, CP) from the slope of the curve and intersection with the y axis, respectively (Figure 7, Table III).

The sintering constant, *k*, was also used to determine the constant of activation, K_a, through equation 4 [15]:

$$K_a = \left(\frac{k\cdot h}{k_B\cdot T}\right) \tag{4}$$

where *k* is the sintering constant, k_B is the Boltzmann constant ($1.381\cdot10^{-23}$ $J\cdot K^{-1}$), *h* is Planck's constant ($6.626\cdot10^{-34}$J) and *T* is the sintering temperature in K.

K_a was related to the Gibbs energy of activation through the van't Hoff Equation [15] in the form of expression (5):

$$\Delta G_a = -R\cdot T\cdot\ln(K_a) \tag{5}$$

Table III summarises the sintering parameters obtained for the different sintering temperatures and microsphere sizes analysed in the present research.

3.4. Bending strength estimation by Gibbs energy of activation, sintering temperature and time

In accordance with the formulae reported above, N_{AREA} can also be expressed in the form of equation 6:

$$N_{AREA} = k\cdot t = \frac{k_B}{h}\cdot t\cdot T\cdot K_a \tag{6}$$

Logarithmic equations obtained from Figure 6 were used to correlate N_{AREA} and experimental bending strength values. In these fitting equations, N_{AREA} was replaced by equation 6 in order to express bending strength as a function of sintering temperature, sintering time and Gibbs energy of activation (equation 7):

$$\sigma_Y = B\cdot\ln(N_{AREA}) + C = B\cdot\ln\left(\frac{k_B\cdot T}{h}\cdot K_a\cdot t\right) + C = B\cdot\ln\left(\frac{k_B}{h}\right) + B\cdot\left[\ln(T\cdot t) - \frac{\Delta G_a}{R\cdot T}\right] + C \tag{7}$$

where coefficients *B* and *C* are obtained from the logarithmic fitting curve in Figure 6. In order to simplify, the constant terms [$B \cdot \ln(k_B/h)$] and *C* were grouped into a new constant term named *P*, giving rise to equation 8. This equation allows bending strength to be estimated when varying the sintering temperature (K), sintering time (seconds) and Gibbs energy of activation (J/mol):

$$\sigma_Y = P + B \cdot \left[\ln(T \cdot t) - \frac{\Delta G_a}{R \cdot T} \right] \quad (8)$$

R being the ideal gas constant. The parameters *P*, *B* and ΔG_a for the microsphere sizes analysed in this paper are reported in Table III. As Figure 8 shows, a good match is observed between values obtained from the model and the experimental ones, meaning that surface area evolution can be used in order to obtain a simple model with which to estimate the evolution of the bending strength of porous samples developed by microsphere sintering. Nevertheless, further research must be conducted in order to validate the accuracy of the fitting parameters obtained in this research. Surface area analysers can be used in order to simplify the process and achieve more accurate results. Again, highest deviations from the model (points marked as empty triangles in Figure 8) correspond to porous samples developed by the sintering of FP microspheres at high temperatures or for long times (i.e. 1673K-8h and 1573K-12h).

4. Discussion

As reported in Table III, the sintering constant, *k*, increases with temperature, which indicates higher kinetic activity and thus a greater development of the sintering necks. For a given sintering temperature, *k* is higher for smaller microspheres, due to their larger specific surface area and, as a consequence, the more energy available during the sintering process [23].

Gibbs energy of activation, ΔG_a, increases with the temperature for every microsphere size and it is almost the same for the smaller particles (FP, MP), while having a higher value for the coarse particles (Table III). This evolution shows that the instability of the transition state increases on raising the temperature or the size of the microspheres, thus promoting a higher development of the sintering necks due to an increase in the sintering rate.

As set out in [19], some reactivity with the underlying alumina of the mould through the yttria coating was observed, especially when sintering the smaller microspheres at higher temperatures or for longer times. This explains the higher deviations observed between the experimental values and those obtained from the model. The mould material was proved to be a critical issue when developing porous Ti6Al4V samples by microsphere sintering, due to the complexity of machining the specimens. Although net-shaped yttria moulds could be used to avoid the undesirable reaction, they are expensive and difficult to produce.

5. Conclusions

A simple model based on the Zero Order Reaction Rate and Transition State Theory has been established in order to evaluate the bending strength of porous Ti6Al4V developed by microsphere sintering. The evolution of the surface area was used to obtain the parameters of the model for three different microsphere sizes. These parameters allow the bending strength variation to be estimated when the sintering temperature and time are

modified and the strength of other microsphere sizes could be easily estimated following this model. Although a good match is observed between data obtained from the model and experimental values, further research must be conducted in order to validate its accuracy. The process can be simplified and more accurate results can be obtained by using surface area analysers in order to determine the evolution of the surface area.

Acknowledgements
The authors are grateful to the Spanish Ministerio de Ciencia e Innovación for supporting this study through project PET2008_0158_02. The translation of this paper was funded by the Universidad Politécnica de Valencia and the Universitat Jaume I.

References
[1] M. WEHMÖLLER, S. WEIHE, C. RASCHE, P. SCHERER, H. EUFINGER, *International Congress series*, 1268, 2004, pp. 667-672.
[2] B. LEVINE, *Adv. Eng. Mater.* 10 (9), 2008, pp. 788-792.
[3] P. TARÍN, *Rev. Metal. Madrid*, 26, 1990, pp. 395-409.
[4] P. C. GARCIA, G. L. ADABO, R. FARIA, S. SOARES, *Dent. Mater.* 22, 2006, pp.1098-1102.
[5] Z. ESEN, S. BOR, *Scripta Materialia*, 56 (5), 2007, pp. 341-344
[6] F. J. GIL, *J. Alloy. Compd.* 439, 2007, pp. 67-73.
[7] K. ASAOKA, M. KON, *Thermec'2003*, PTS 1-5, 426-4, 2003, pp. 3079-3084.
[8] M. NIINOMI, *J. Mech. Behav. Biomed. Mater.* 1, 2008, pp. 30-42.
[9] M. YSANDER, *J. Rehabil. Res. Dev.* 38, 2001, pp. 183-190.
[10] N. NOMURA; T. KOHAMA; I.H. OH; S. HANADA; A. CHIBA; M. KANEHIRA; K. SASAKI, *Mater. Sci. and Eng. C* 25, 2005, pp. 330-335.
[11] M. BRAM, H. SCHIEFER, BOGDANSKI, M. KOLLER, H.P. BUCHKREMER, D. STOVER, *Euro PM2005, PM Applications*, 2005, pp. 517-522.
[12] H. J. RACK, J. I. QAZI, *Mater. Sci. Eng. C* 26-8, 2006, pp. 1269-1277.
[13] D. KUPP, D. CLAAR, K. FLEMMIG, U. WAAG, GOEHLER H., *Processing and properties of lightweight cellular metals and structures*, Seattle, Washington, February 17-21, 2002, pp. 61-71.
[14] A. BANSIDDHI, T.D. SARGEANT, S.I. STUPP, D.C. DUNAND, *Acta Biomater.* 4, 2008, pp. 773-782.
[15] Y. SARIKAYA, K. ADA, M. ÖNAL, *J. Alloy. Compd.* 432-1/2, 2007, pp. 194-199.
[16] M. SAITOU, *Philos. Mag. Lett.* 80, 2000, pp. 755-761.
[17] A. L. MAXIMENKO, E. A. OLEVSKY, *Acta Mater.* 52, 2004, pp. 2953-2963.
[18] A. K. BURNHAM, *Chem. Eng. J.* 108, 2005, pp. 47-50.
[19] L. REIG, V. AMIGO D.J. BUSQUETS, J.A. CALERO, J.Mater.Process.Technol., 2011, DOI.10.1016/j.jmatprotec.2011.06.026
[20] V. AMIGÓ, L. REIG, D. BUSQUETS D., *EUROMAT2007*, Nürnberg, Germany, 2007.
[21] D. BUSQUETS-MATAIX, L. REIG, V. AMIGÓ, J.A. CALERO, *Euro PM2008*, Proceedings v.02, 2008.
[22] M. F. ASHBY, K. JOHNSON, *Materials and Design: The Art and Science of Material Selection in Product Design*, second ed., Butterworth-Heinemann, 2003, pp. 117-140.
[23] R.M. GERMAN, *Powder metallurgy and particulate materials processing: the processes, materials, products, properties and applications*, Metal Powder Industries Federation, 2005.

Fig 1.Particle size distribution of Ti64 microspheres

Click here to download high resolution image

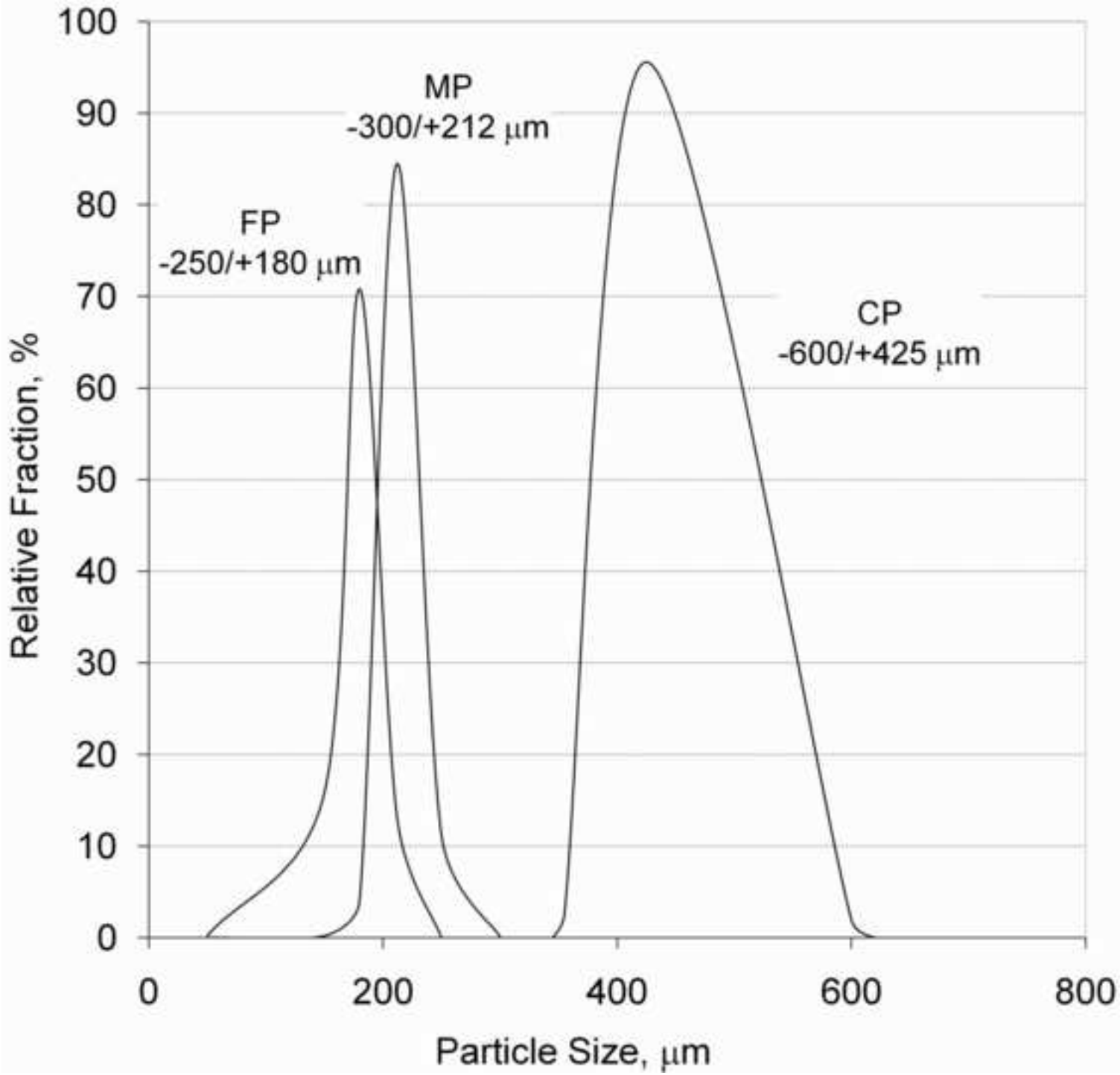

Fig 2. SEM Micrograph image of fine particle size microspheres.
Click here to download high resolution image

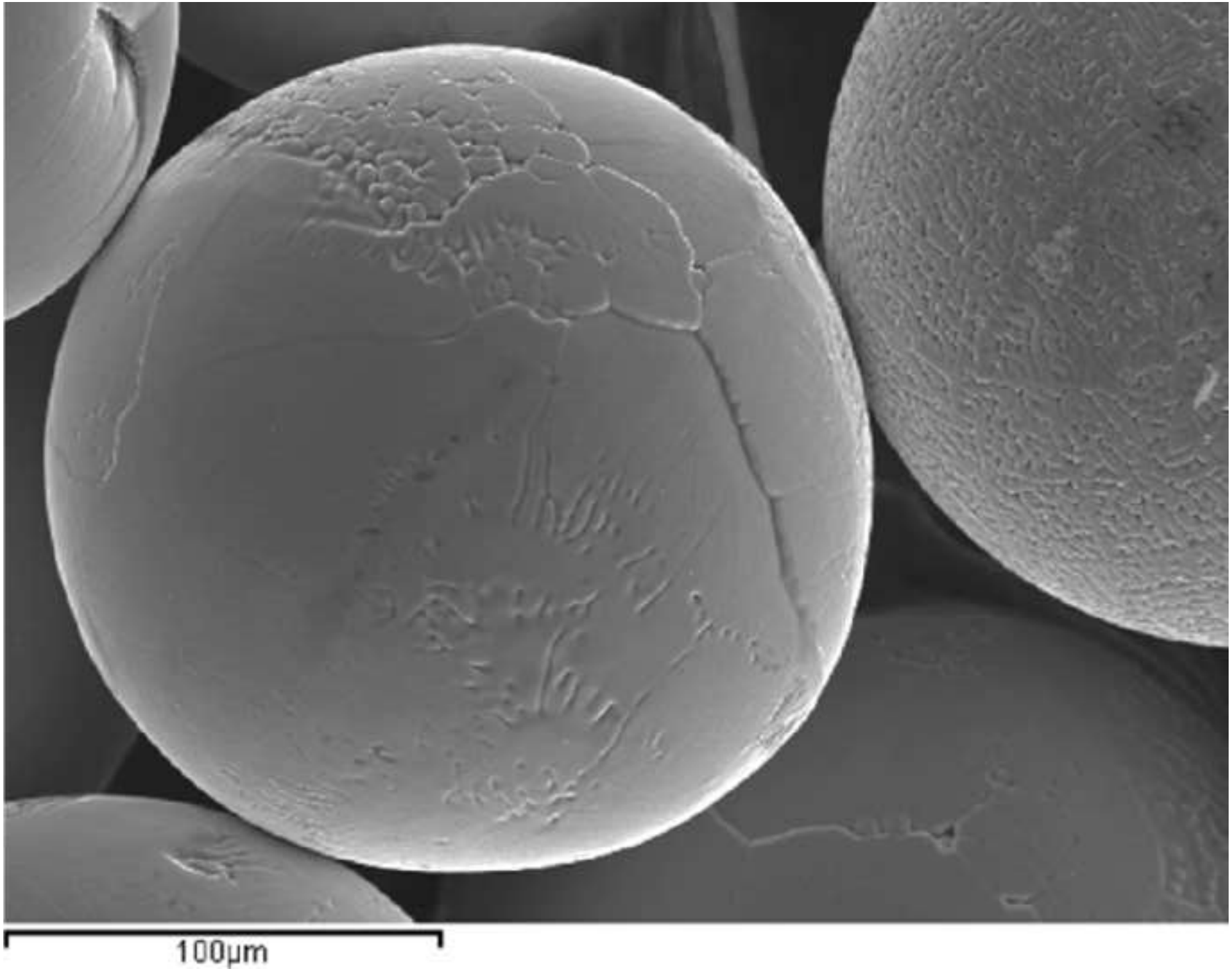

Fig 3. SEM image of the sinter neck areas formed during sinter.
Click here to download high resolution image

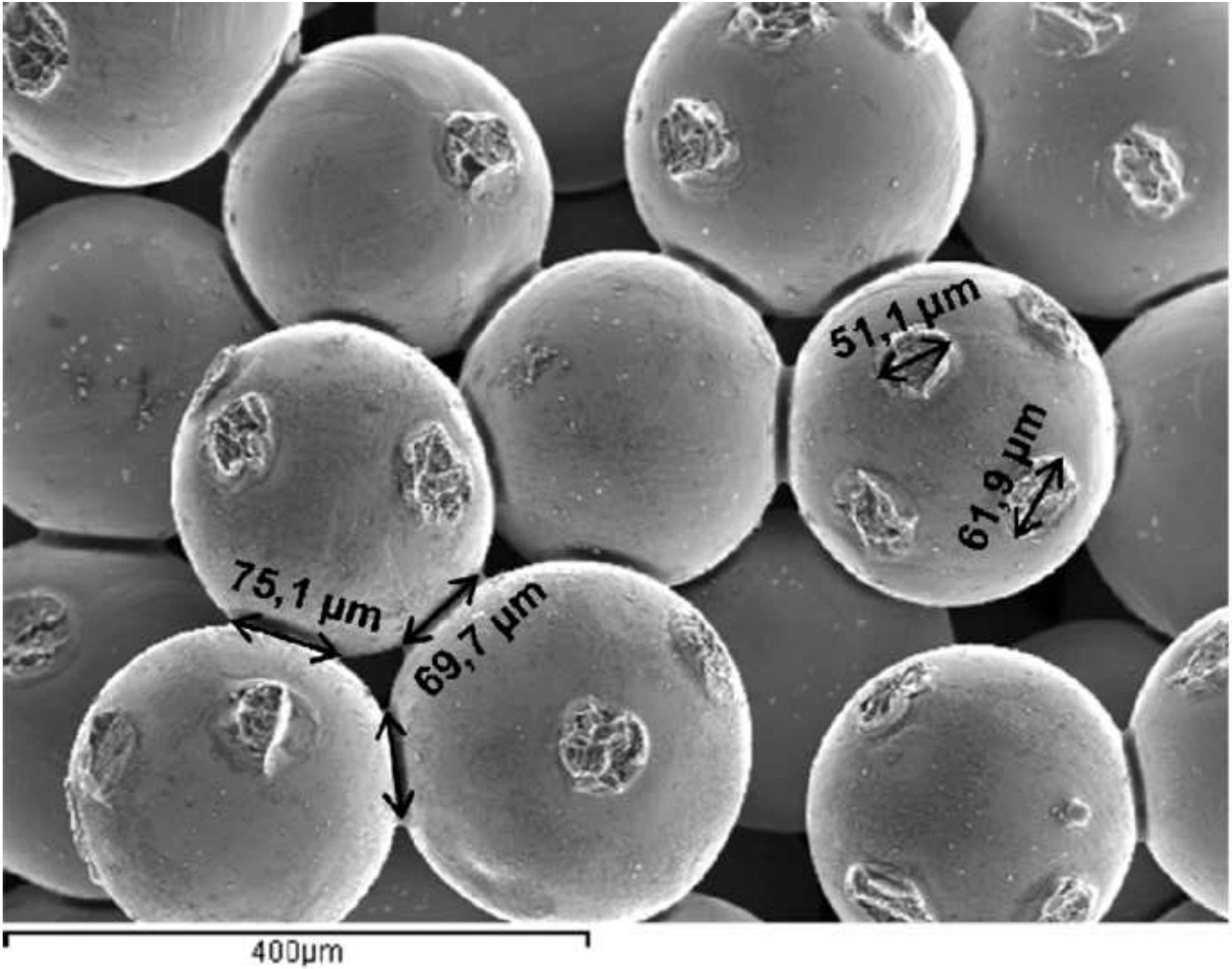

Fig.4. Average diameter sinter neck developed for each size & T

Click here to download high resolution image

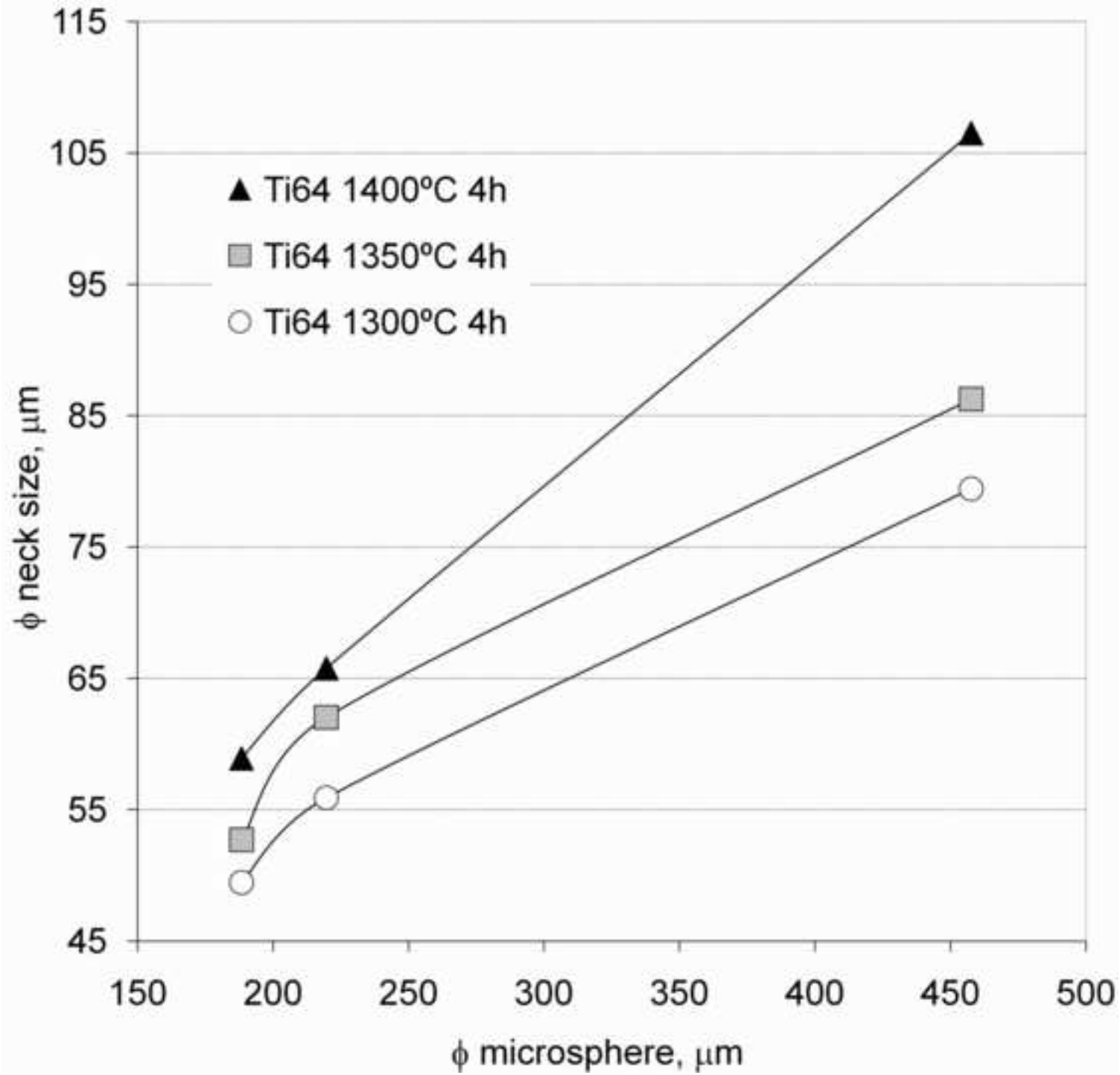

Fig 5a. Neck area developed by fine ME versus t and T

Click here to download high resolution image

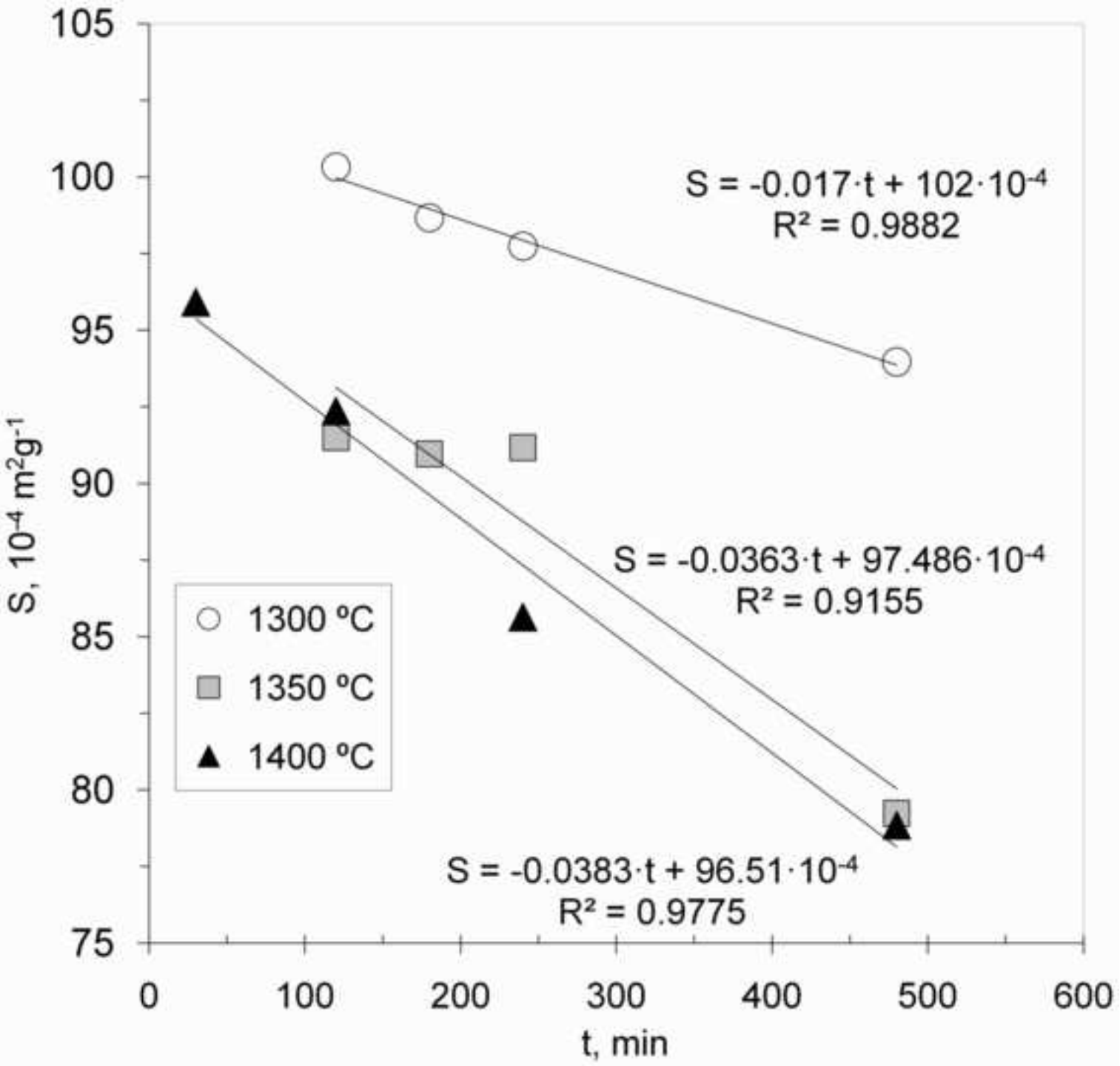

Fig 5b. Neck area developed by medium ME versus t and T

Click here to download high resolution image

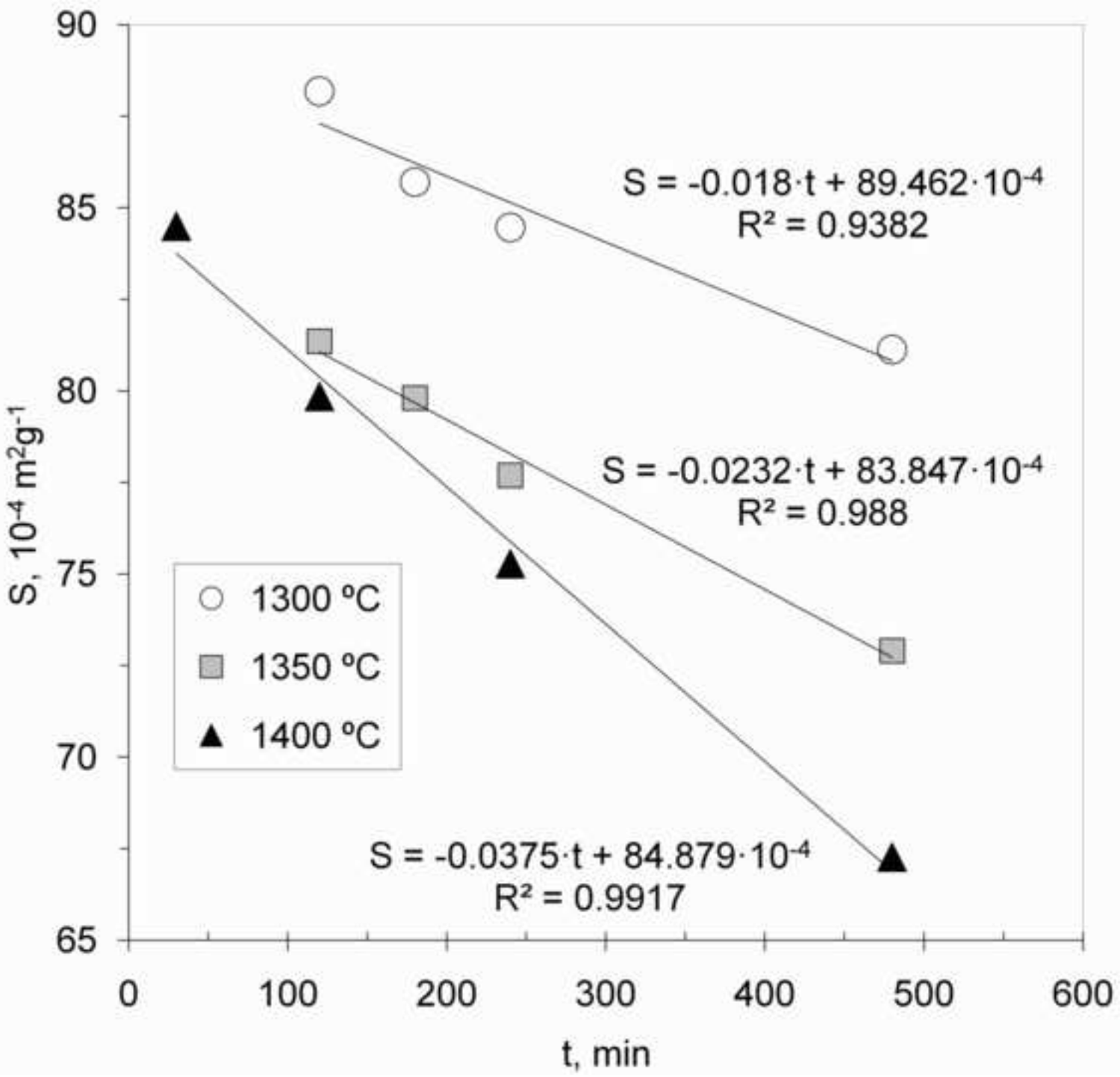

Fig 5c. Neck area developed by coarse ME versus t and T

Click here to download high resolution image

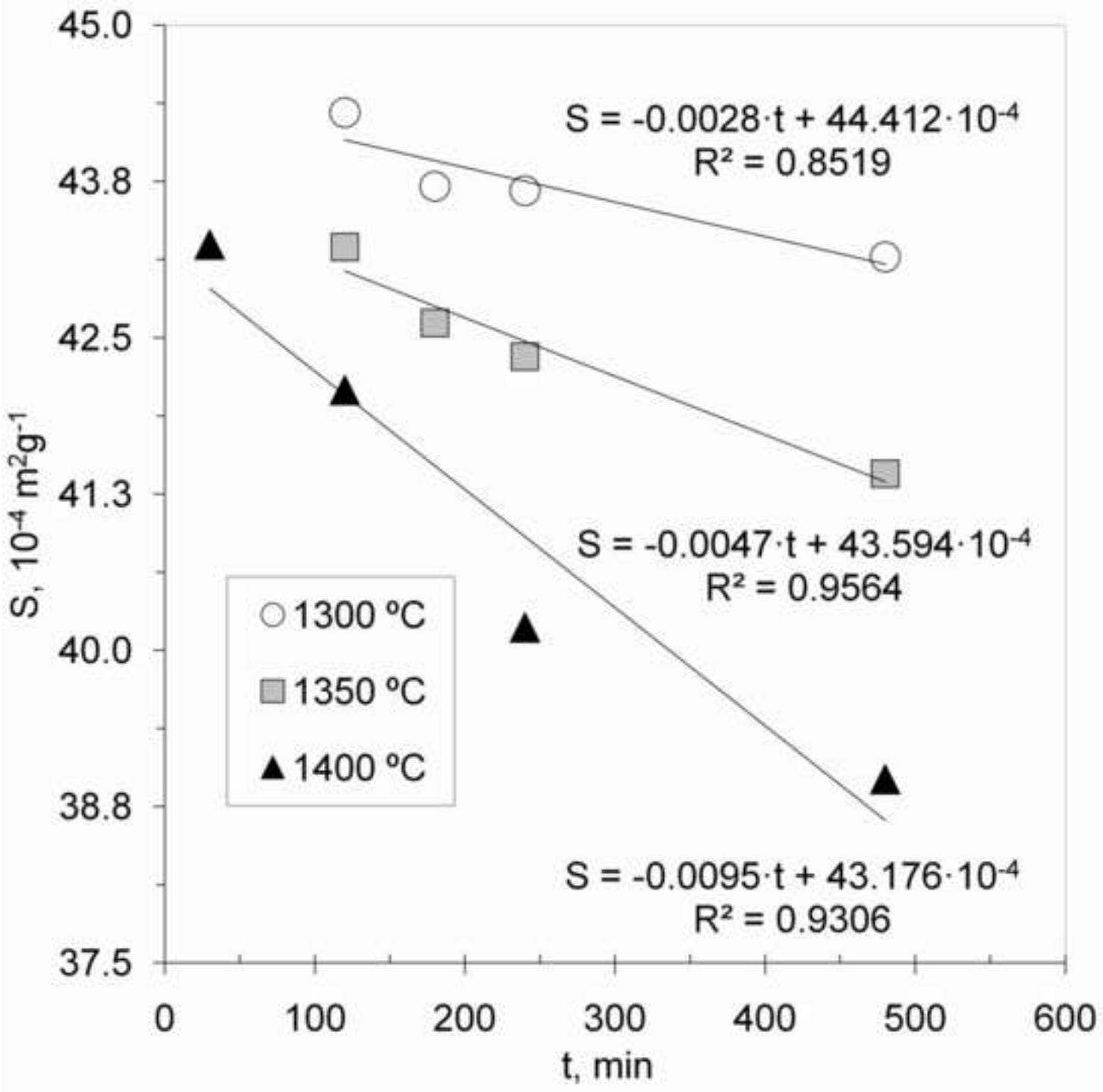

Fig 6. Correlation neck area by model & bending strength

Click here to download high resolution image

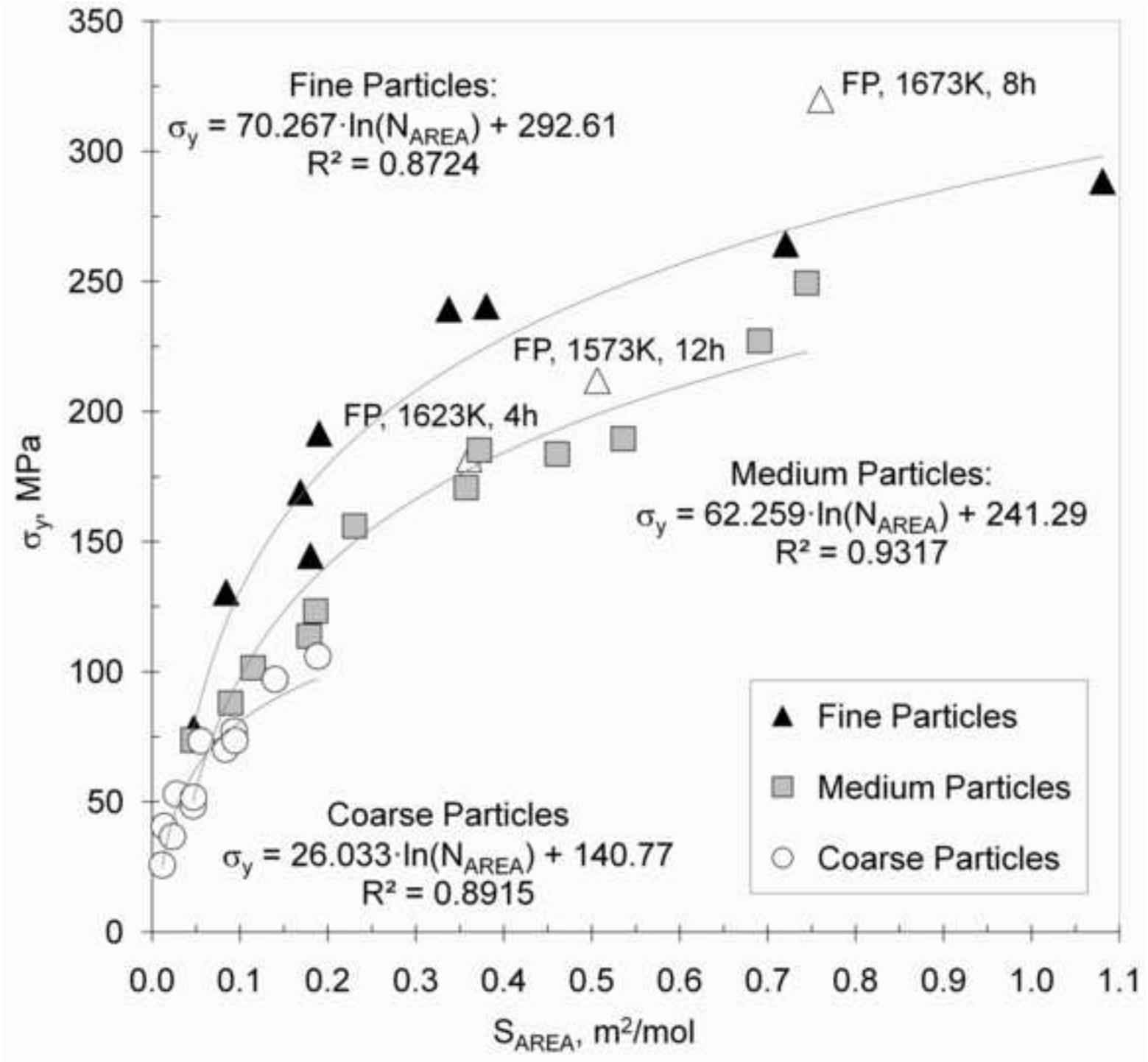

Fig 7. Arrhenius equation applied to the sintering of Ti6Al4V ME

Click here to download high resolution image

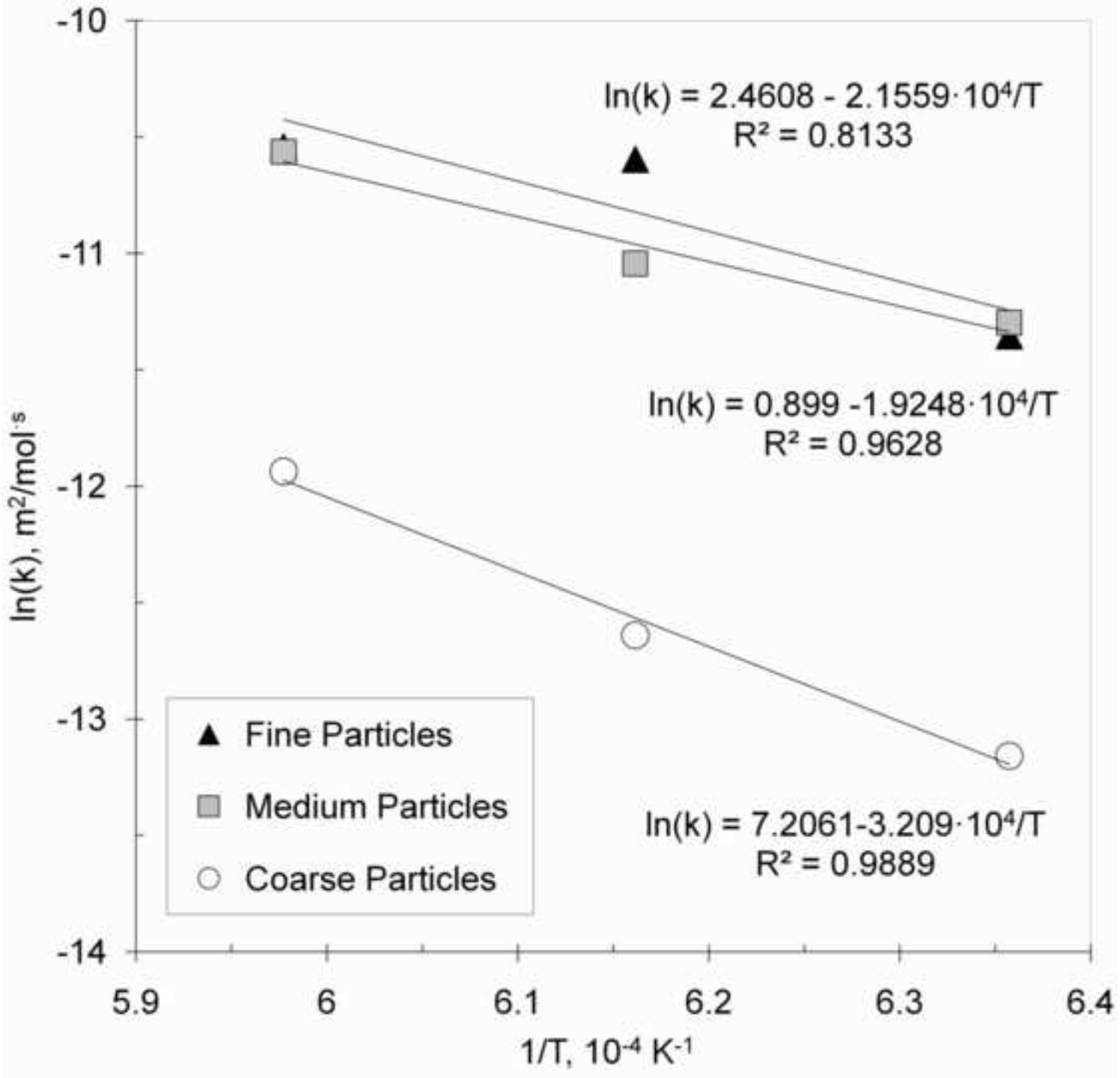

Fig 8. Correlation bending strength experimental & model

Click here to download high resolution image

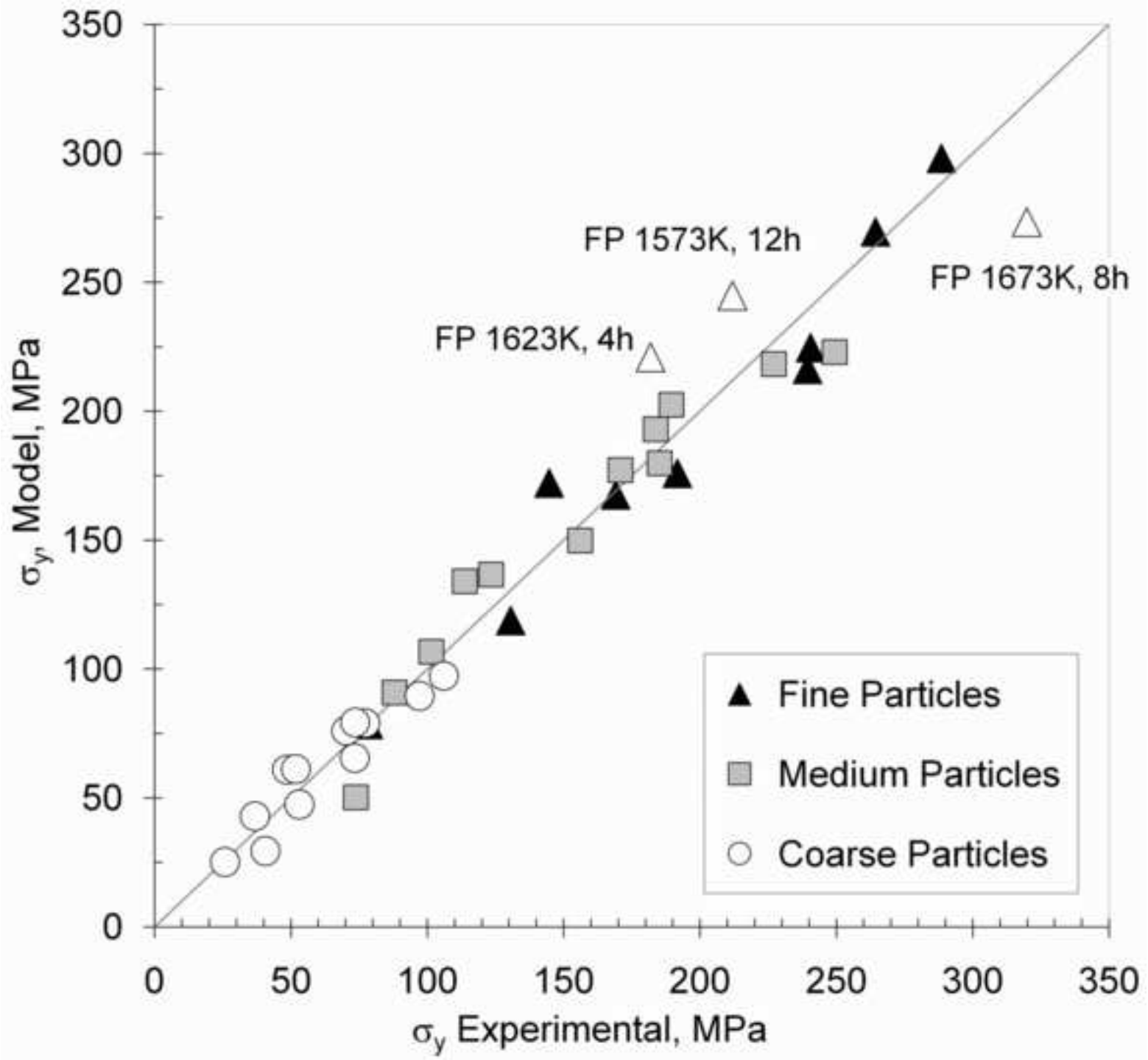

Table I Rewied

Table I. Chemical composition of the Ti6Al4V, %Wt, microspheres supplied by Phelly Materials compared to ASTM F1580-01 standards.

Element	Al	V	O	Fe	C	H	N	Cu	Sn	Ti
ASTM F1580-07	5.5-6.75	3.5-4.5	0.20	0.30	0.08	0.015	0.05	0.1	0.1	Balance
FP	6.45	4.15	0.12	0.13	0.041	0.004	0.029	<0.05	<0.05	Balance
MP	6.73	4.05	0.11	0.21	0.016	0.004	0.026	<0.1	<0.1	Balance
CP	6.15	4.18	0.076	0.072	0.016	0.002	0.006	<0.01	<0.01	Balance

Table II. Evolution of free surface area ($\Delta S/S_0$) for the different microsphere sizes at different sintering temperatures and times.

t, min	Particle size	T, K		
		1573	1623	1673
30	FP			0.15
	MP			0.13
	CP			0.07
120	FP	0.12	0.19	0.19
	MP	0.09	0.16	0.18
	CP	0.05	0.07	0.09
240	FP	0.14	0.20	0.24
	MP	0.13	0.20	0.22
	CP	0.06	0.09	0.14
480	FP	0.17	0.30	0.30
	MP	0.16	0.25	0.31
	CP	0.07	0.11	0.16
720	FP	0.23	0.36	
	MP	0.16	0.26	
	CP	0.09	0.11	

Table III. Model parameters obtained from the ZORR model and TST applied to porous Ti64 specimens developed by microsphere sintering.

ME size	T, K	S_0, m^2g^{-1}	k 10^{-6}, $m^2g^{-1}min^{-1}$	Ln (A)	A	Ea/R	E_a, $J{\cdot}mol^{-1}$	B	C	P	ΔG_a, $J{\cdot}mol^{-1}$
FP	1573	0.0102	1.70	2.461	11.71	$2.156{\cdot}10^4$	179,241	70.267	292.61	1962.17	555,490
	1623	0.0097	3.63								563,333
	1673	0.0097	3.83								580,364
MP	1573	0.0089	1.80	0.899	2.46	$1.925{\cdot}10^4$	160,028	62.259	241.29	1720.58	554,743
	1623	0.0084	2.32								569,374
	1673	0.0085	3.75								580,685
CP	1573	0.0044	0.28	7.2061	1347.6	$3.209{\cdot}10^4$	266,796	26.033	140.77	759.32	579,078
	1623	0.0044	0.47								590,918
	1673	0.0043	0.95								599,756

Supplementary Data

Click here to download Supplementary Data: PT_List of figures and Tables.doc